AIChE

# Permeation Model and Experimental Investigation of Mixed Conducting Membranes

**Xuefeng Zhu, Huanying Liu, You Cong, and Weishen Yang**
State Key Laboratory of Catalysis, Dalian Institute of Chemical Physics, Chinese Academy of Sciences, Dalian, China

*DOI 10.1002/aic.12710*
*Published online July 27, 2011 in Wiley Online Library (wileyonlinelibrary.com).*

*A simple oxygen permeation model was developed based on the theoretical analysis of the role of interfaces of mixed conducting membranes. The developed model equations contain three resistance constants, which can be determined by correlating oxygen permeation flux to oxygen partial pressure on each side. A series of experimental measurements of oxygen fluxes of $Ba_{0.5}Sr_{0.5}Co_{0.8}Fe_{0.2}O_{3-\delta}$ membranes over a wide range of temperature and oxygen partial pressures were tested for the regression of three resistance constants with good correlation ($R > 0.997$). With this model, the interfacial exchange resistances of each side can be well distinguished from the bulk-diffusion resistance under a wide-temperature range. The kinetics parameters, including interfacial exchange coefficients on each side and ionic diffusion coefficient, can be obtained through the three resistance constants. Parametric studies can predict the influences of membrane thickness, oxygen partial pressures on oxygen flux, distribution of permeation resistances, and characteristic thickness.* © 2011 American Institute of Chemical Engineers *AIChE J,* 58: 1744–1754, 2012
*Keywords: interfacial exchange, bulk diffusion, MIEC membrane, oxygen permeation, distribution of resistances*

## Introduction

Mixed ionic–electronic conducting (MIEC) membranes, made of perovskite-type and/or fluorite-type oxides, can separate oxygen from air at elevated temperature with infinite permeation selectivity.[1–3] The MIEC materials can be applied potentially in the field of oxygen separation, solid oxide fuel cells (SOFCs),[4–6] membrane reactors for the partial oxidation of light hydrocarbons,[7–10] oxy-fuel process for $CO_2$ capture, and so on.[11,12]

Oxygen permeation fluxes through MIEC membranes can be well described by the Wagner equation, which assumes the bulk diffusion to be the rate determining step (r.d.s.).[13] If the dipole conductivity is marginally affected by oxygen partial pressure across membranes, the equation shows a simple dependence of oxygen flux on the operating temperature and oxygen partial pressure. However, only few membranes or membranes with sufficient thickness can meet the requirement of bulk-diffusion limitation. To achieve practical and effective applications of MIEC membranes, it is necessary to understand the oxygen permeation mechanism and know the r.d.s in the oxygen transport process.

Except for bulk diffusion, there are two potential r.d.s involved in the oxygen permeation across a dense MIEC membrane. They are the oxygen exchange at the gas–solid interface of the feed side and the permeation side, as shown in Figure 1. The exchange process between gas phase oxygen molecules and solid membrane surfaces includes a series of reaction steps, and every of these steps may play important roles in oxygen permeation through membranes. Elemental steps, like adsorption, dissociation, charge transfer, surface diffusion, and oxygen ions merging into lattices, are involved on the interfacial zone of the feed side. The same elemental steps occur on the interfacial zone of permeation side but in the reverse direction. The overall reactions can be written as

$$\frac{1}{2}O_2 + V_O^{\bullet\bullet} \rightleftharpoons O_O^x + 2h^{\bullet} \quad (1)$$

The interfacial exchange reactions on both sides become the r.d.s. in oxygen permeation, if the bulk transport is fast enough compared with the exchange reactions. The Wagner equation can well describe the dependence of oxygen permeation flux on operating temperature and oxygen partial pressure gradients, if the bulk diffusion is the r.d.s. However, for most MIEC membranes, the oxygen permeation process is jointly controlled by the bulk diffusion and interfacial exchanges and sometimes mainly limited by interfacial exchanges. Under these circumstances, the Wagner equation is ineffective to describe the permeation flux.

Jacobson and coworkers derived a general equation to describe oxygen permeation through MIEC membranes based on the dependence of net oxygen interfacial exchange flux under a chemical potential of the gas and the ion–electron holes at the gas/solid interface.[14–16] However, the equation is complicated when oxygen permeation is jointly controlled by interfacial exchange and bulk diffusion and cannot show clearly the dependence of the flux on temperature and oxygen partial pressure across membranes. Another general equation was developed by Xu and Thomson, who simplified Lin's

Correspondence concerning this article should be addressed to X. Zhu at zhuxf@dicp.ac.cn or W.S. Yang at yangws@dicp.ac.cn.

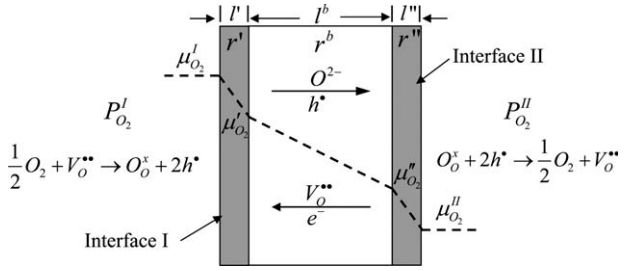


**Figure 1. Schematic graph of oxygen chemical potential drop across a MIEC membrane.**

model by analyzing the diffusion of oxygen vacancies through membranes and the oxygen exchange reactions at the interfaces.[17,18] Three permeation resistances can be determined by the regression analysis of their model parameters, and a clear map can be easily drawn to show how the temperature and oxygen pressure affect the distribution of permeation resistances. In developing their model, four assumptions were proposed: (1) the electronic conductivity is much greater than the ionic conductivity; (2) the diffusion coefficient of oxygen vacancies does not change with oxygen pressure; (3) the forward and reverse reactions have the same rate constant, and (4) the law of mass action can be used for the oxygen exchange reactions on both sides. However, some membrane materials cannot satisfy all these assumptions; especially, it is not the case that the forward and reverse reactions have the same rate constant for many perovskite oxides.

In this article, an explicit oxygen permeation model is developed for MIEC membranes based on the theoretical analysis by Virkar.[19] In this model, the distribution of two interfacial resistances and bulk resistance can be properly addressed to show the effects of temperature, oxygen partial pressures over both sides and membrane thickness on the oxygen permeation process.

## Theory

The role of interfaces in the oxygen transport through MIEC membranes has been discussed in detail,[19] here, a brief introduction of the analysis was presented. Appropriate assumptions are necessary to allow for the theoretical analysis, development of simple equations and understanding the nature of interface effects. The following three assumptions are proposed: (1) The transport properties of electrons/holes and oxygen ions in a given zone are constants regardless of position and oxygen chemical potentials. (2) The diffusion resistance or concentration polarization resistance for oxygen molecules transporting from the environmental atmosphere to the membrane interfaces on both sides can be totally ignored. It should be noted that this hypothesis may be invalid for thin membranes with thick supports. (3) All the steps, including adsorption, dissociation, charge transfer, surface diffusion, and oxygen ions merging into lattices, take place under isothermal conditions.

For a mixed electronic–ionic conductor, the equilibrium of interest is the following

$$\tfrac{1}{2}O_2 + 2e' \leftrightarrow O^{2-} \tag{2}$$

And at thermodynamic equilibrium, the oxygen exchange current density from the gas to the solid is equal to that from the solid to the gas. Also, the following relationship should be satisfied

$$\tfrac{1}{2}\mu_{O_2} + 2\mu_e = \mu_{O^{2-}} \tag{3}$$

For small deviations from the thermodynamic equilibrium, one can expand Eq. 3 to give

$$\tfrac{1}{2}\delta\mu_{O_2} + 2\delta\mu_e = \delta\mu_{O^{2-}} \tag{4}$$

where $\delta X$ denotes a small deviation in the thermodynamic potential $X$ from the equilibrium state. Local equilibrium needs to be kept, and this requires that the membrane material can transport at least two kinds of species in and out. For mixed conducting materials, fast transport of both electrons and oxide ions makes it easy to maintain local equilibrium. Oxygen ionic and electronic current densities are given by

$$I_{O^{2-}} = \frac{\sigma_{O^{2-}}}{2F}\nabla\mu_{O^{2-}} = \frac{\sigma_{O^{2-}}}{2F}\frac{d\mu_{O^{2-}}}{dx} \tag{5}$$

and

$$I_e = \frac{\sigma_e}{F}\nabla\mu_e = \frac{\sigma_e}{F}\frac{d\mu_e}{dx} \tag{6}$$

Substituting Eq. 4 into Eq. 5, we can get the following relationship

$$I_{O^{2-}} = \frac{\sigma_{O^{2-}}}{4F}\frac{d\mu_{O_2}}{dx} + \frac{\sigma_{O^{2-}}}{F}\frac{d\mu_e}{dx} \tag{7}$$

Figure 1 shows a schematic illustration of a mixed conducting membrane across which exists an oxygen chemical potential difference ($\mu^{I}_{O_2} - \mu^{II}_{O_2}$) and an electronic chemical potential difference ($\mu^{I}_{e} - \mu^{II}_{e}$). Transport of oxygen ions and electrons happens across the interfacial zones, which can be greatly affected by external conditions. Therefore, the thicknesses of the interfacial zones are difficult to determine and not very well defined either. Virkar assumed that the "interfacial zones" are of a certain thickness and used the assumption to describe transport properties through both interfacial zones in terms of conductivity and thickness.[19] $\sigma'_{O^{2-}}$, $\sigma'_e$, $\sigma''_{O^{2-}}$ and $\sigma''_e$ are the oxygen ionic and electronic conductivities at interfacial zones I and II, respectively. $l'$ and $l''$ are the thickness of interfacial zones I and II, respectively. The specific conductance (S $cm^{-2}$) and specific resistance ($\Omega$ $cm^2$) are introduced, because it is impossible to separately determine conductivities and the thickness of interfacial zones, however, specific conductance and resistance can be measured experimentally. As an example, the following relationship describes the specific oxygen ionic conductance and resistance of interfacial zone I

$$\kappa'_{O^{2-}} = \frac{\sigma'_{O^{2-}}}{l'} = \frac{1}{r'_{O^{2-}}} \tag{8}$$

The equation is based on the simple assumption that the transport properties are constants across the interfacial zones. The interfacial oxygen ionic or electronic conductivity is not equal to the conductivity in the bulk membrane, because it is greatly influenced by microstructure, interfacial elemental composition, and so on. Based on the assumption of homogeneous transport properties across the interfacial zones, the oxygen ionic and electronic current densities are given by

$$I'_{O^{2-}}=\frac{\kappa'_{O^{2-}}}{4F}(\mu'_{O_2}-\mu^{I}_{O_2})+\frac{\kappa'_{O^{2-}}}{F}(\mu'_{e}-\mu^{I}_{e})=\frac{\mu'_{O_2}-\mu^{I}_{O_2}}{4Fr'_{O^{2-}}}+\frac{\mu'_{e}-\mu^{I}_{e}}{Fr'_{O^{2-}}} \tag{9}$$

and

$$I''_{O^{2-}}=\frac{\kappa''_{O^{2-}}}{4F}(\mu^{II}_{O_2}-\mu''_{O_2})+\frac{\kappa''_{O^{2-}}}{F}(\mu^{II}_{e}-\mu''_{e})=\frac{\mu^{II}_{O_2}-\mu''_{O_2}}{4Fr''_{O^{2-}}}+\frac{\mu^{II}_{e}-\mu''_{e}}{Fr''_{O^{2-}}} \tag{10}$$

By analogy with oxygen ionic current densities through the two interfacial zones, the electronic current densities can be written as

$$I'_{e}=\frac{\kappa'_{e}}{F}(\mu'_{e}-\mu^{I}_{e})=\frac{\mu'_{e}-\mu^{I}_{e}}{Fr'_{e}} \tag{11}$$

and

$$I''_{e}=\frac{\kappa''_{e}}{F}(\mu^{II}_{e}-\mu''_{e})=\frac{\mu^{II}_{e}-\mu''_{e}}{Fr''_{e}} \tag{12}$$

In the above equations, $\mu'_{O_2}$, $\mu'_{e}$, $\mu''_{O_2}$ and $\mu''_{e}$ are the oxygen chemical potential and electronic chemical potential at interfaces I and II, respectively. For mixed conducting membranes, when the oxygen permeation reaches a steady state, the oxygen ionic current densities in both interfacial zones are equal to each other, so do the electronic current densities. There is no differentiation any more, therefore, $I_{O^{2-}}$ and $I_e$ will be used to denote the oxygen ionic and electronic current densities, respectively. As there is no voltage is applied to the MIEC membranes and only an oxygen chemical potential gradient imposed across the membranes, the net current through the membranes is zero, that is $I_{O^{2-}}+I_e=0$. Furthermore, $I_{O^{2-}}<0$ and $I_e>0$. By combining Eqs. 9 and 11 and Eqs. 10 and 12, respectively, and rewriting the equations, one can obtain expressions for the oxygen chemical potentials at the interfaces

$$\mu'_{O_2}=\mu^{I}_{O_2}-4F(r'_{O^{2-}}+r'_{e})|I_{O^{2-}}| \tag{13}$$

$$\mu''_{O_2}=\mu^{II}_{O_2}+4F(r''_{O^{2-}}+r''_{e})|I_{O^{2-}}| \tag{14}$$

For a membrane in the bulk-diffusion zone, the oxygen ionic and electronic conductivities of the membrane are supposed not to change along with the decrease of oxygen chemical potential, or under a small gradient of oxygen chemical potential, the oxygen permeation flux can be written as

$$j_{O_2}=-\frac{1}{4^2F^2l^b}\frac{\sigma^{b}_{O^{2-}}\sigma^{b}_{e}}{\sigma^{b}_{O^{2-}}+\sigma^{b}_{e}}\ \Delta\mu^{b}_{O_2}=-\frac{1}{4^2F^2}\frac{1}{r^{b}_{O^{2-}}+r^{b}_{e}}\Delta\mu^{b}_{O_2} \tag{15}$$

where $\sigma^{b}_{O^{2-}}$, $\sigma^{b}_{e}$, and $\Delta\mu^{b}_{O_2}$ are the oxygen ionic conductivity, electronic conductivity and oxygen chemical potential difference in the bulk-diffusion zone, respectively; $l^b$ is the thickness of the bulk-diffusion zone. Considering $|I_{O^{2-}}|=4Fj_{O_2}$, and substituting this equation into Eq. 15, one obtains an equation about the gradient of oxygen chemical potential in the bulk-diffusion zone

$$\Delta\mu^{b}_{O_2}=\mu'_{O_2}-\mu''_{O_2}=4F|I_{O^{2-}}|(r^{b}_{O^{2-}}+r^{b}_{e}) \tag{16}$$

Subtracting Eq. 14 from Eq. 13 and combining the result with Eq. 16 gives the equation

$$(\mu^{I}_{O_2}-\mu^{II}_{O_2})=4F|I_{O^{2-}}|(r'_{O^{2-}}+r'_{e})+4F|I_{O^{2-}}|(r^{b}_{O_2}+r^{b}_{e})+4F|I_{O^{2-}}|(r''_{O^{2-}}+r''_{e}) \tag{17}$$

where the formula on the left side is the total oxygen chemical potential difference across the membrane; the formulae on the right side are the reduced oxygen chemical potential at interface I, the reduced oxygen chemical potential in the bulk-diffusion zone, and the reduced oxygen chemical potential at interface II, so the available total driving force is distributed in three parts across the membrane

$$\Delta\mu^{tot}_{O_2}=\Delta\mu'_{O_2}+\Delta\mu^{b}_{O_2}+\Delta\mu''_{O_2} \tag{18}$$

A general transport equation derived from Eq. 18 gives

$$j_{O_2}=-\frac{1}{4^2F^2}\frac{1}{r'+r^{b}+r}\Delta\mu^{tot}_{O_2}=-\frac{\Delta\mu^{tot}_{O_2}}{4^2F^2}\frac{1}{r^{tot}} \tag{19}$$

where $-\Delta\mu^{tot}_{O_2}/4^2F^2$ is the total driving force across the membrane. $r^{tot}=r'+r^{b}+r''$ is the total permeation resistance, and can be calculated from the following equations

$$r^{tot}=-\frac{\Delta\mu^{tot}_{O_2}}{4^2F^2j_{O_2}}=-\frac{RT}{4^2F^2j_{O_2}}\ln\frac{P^{II}_{O_2}}{P^{I}_{O_2}} \tag{20}$$

In general, the specific resistances of the interfacial regions are functions of oxygen partial pressure. Usually, a simply power function can been used to describe the relationship between interface specific resistance and the oxygen partial pressure;[19] therefore, we can obtain the following relationship

$$r'=r'_0(P^{I}_{O_2}/P_0)^{-\frac{1}{n}} \tag{21}$$

and

$$r''=r''_0(P^{II}_{O_2}/P_0)^{-\frac{1}{n}} \tag{22}$$

where $P_0$, $r'_0$, and $r''_0$ are the oxygen partial pressure of 1 bar, area specific resistances of the feed side and permeation side at oxygen partial pressure of 1 bar, respectively. $n$ is a positive number, typically an integer. Under conditions close to thermodynamic equilibrium, the permeation flux through an interface can be described as[13]

$$j_{O_2}=-j_{ex}\frac{\Delta\mu_{O_2}}{k_BT} \tag{23}$$

where $j_{ex}$ is the balance exchange rate in the absence of oxygen potential gradients at the interface. In the simplest cases, the latter quantity is directly related to the equilibrium interfacial exchange coefficient $k_{ex}$, which can be obtained from experimental data of $^{18}O$—$^{16}O$ isotopic exchange[13]

$$j_{ex}=1/4k_{ex}C_{O^{2-}} \tag{24}$$

where $C_{O^{2-}}$ (mol m$^{-3}$) is the volume concentration of oxygen anions at equilibrium. Therefore, by combining Eqs. 23, 24, and the relationship $|I_{O^{2-}}|=4Fj_{O_2}$, the real exchange coefficient at interface I gives

$$k'_{ex}=\frac{RT}{4F^2C'_{O^{2-}}}\frac{1}{r'} \tag{25}$$

Experimental and theoretical investigations reveal that the equilibrium interfacial exchange coefficient is a function of oxygen partial pressure

$$k_{ex} = k_0 \left( \frac{P_{O_2}}{P_0} \right)^{0.5} \tag{26}$$

where $k_0$ is the equilibrium interfacial exchange coefficient at oxygen partial pressure of 1 bar. Therefore, combining Eqs. 25 and 26, and considering that the concentration of oxygen ions at the interfacial zone is almost a constant over a small oxygen pressure range, one can derive that the value of n in Eqs. 21 and 22 is 2. In addition, over a small oxygen pressure range, the influence of the oxygen partial pressure on the membrane bulk resistance (including electronic resistance and ionic resistance) can be ignored without inducing significant error. Therefore, one can get the following two relationships

$$r^{tot} = r_0'(P^{I}_{O_2}/P_0)^{-\frac{1}{2}} + (r^b + r'') \tag{27}$$

and

$$r^{tot} = r_0''(P^{II}_{O_2}/P_0)^{-\frac{1}{2}} + (r^b + r') \tag{28}$$

The total specific resistance can be calculated from Eq. 20, and if the oxygen pressure on the permeation side is fixed and on feed side is varied, one can obtain $r_0'$ and $r^b + r''$ through linear regression. Similarly, $r_0''$ and $r^b + r'$ can be obtained through linear regression of Eq. 28.

Bouwmeester and Burggraaf introduced the characteristic thickness, $L_c$, to define the membrane thickness corresponding to the transition from predominantly controlled by bulk diffusion to the state when permeation is mainly governed by the interfacial exchange.[13,20]

$$L_c = \frac{D_s}{k_{ex}} = \frac{D^*}{k_{ex}} \tag{29}$$

and

$$D_s = \frac{\sigma^b_{O^{2-}} RT}{4F^2 C_{O^{2-}}} \tag{30}$$

where $D_s$ is the self-diffusion coefficient of oxygen ions derived from the classical Nernst–Einstein relationship, and $D^*$ is the tracer diffusion which coefficient equals to the self-diffusion coefficient, if correlation effects can be neglected. The above equations are simplified and only valid for small oxygen partial pressure gradients applied across membranes, and under the condition that the concentration of oxygen ions in oxides can be treated as constants. Considering that both interfacial exchange processes make contributions to the characteristic thickness, a combined oxygen exchange coefficient is defined as

$$k^{tot}_{ex} = k'_{ex} k''_{ex} / (k'_{ex} + k''_{ex}) \tag{31}$$

Combining Eqs. 25, 29, and 31, and assuming $l', l'' << l^b \approx L$, one can obtain the following relationship

$$L_c = \frac{r' + r''}{r^b} L \tag{32}$$

Therefore, it can be found that $L_c$ is a process parameter which changes with oxygen partial pressure on both sides of membranes. Also, the relationship reveals that at the characteristic thickness the bulk-diffusion resistance equals to the total interfacial exchange resistance.

In this article, $Ba_{0.5}Sr_{0.5}Co_{0.8}Fe_{0.2}O_{3-\delta}$ (BSCF) was investigated to determine the distribution of permeation resistance across the membranes using the above theoretical model. The effects of temperature, oxygen partial pressure on both sides, and membrane thickness were considered.

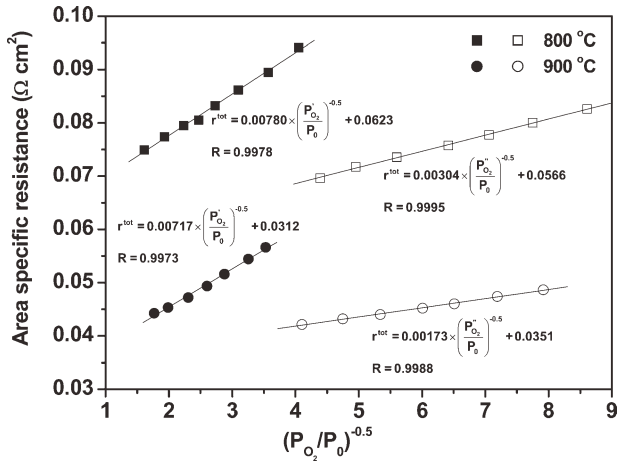


**Figure 2. Dependence of total permeation resistance on oxygen partial pressure of each side for a 0.5-mm BSCF membrane.**

**Solid symbols: varying the oxygen partial pressure of feed side; open symbols: varying the oxygen partial pressure of permeation side.**

## Experimental

BSCF composite oxide powder was synthesized via the ethylenediamine tetraacetic acid (EDTA)–citric acid complex method, and the detail procedure was described in the literature.[21–23] The composite oxide powder was then pressed and sintered at appropriate temperatures.[21] After being polished by 800 mesh SiC papers to the required thickness, the disks were sealed by silver rings at its melting point. The procedures of oxygen permeation testing were the same as previous reports.[21–23] Oxygen partial pressures in the feed were adjusted by changing the flow rates of pure oxygen and pure nitrogen and controlled in the range of 0.07–0.4 bar. The flow rate of synthesized air was 200–300 mL $min^{-1}$. Oxygen partial pressures of the permeation side were adjusted by changing the flow rate of sweeping gas (helium) and controlled in the range of 0.005–0.05 bar, corresponding to the helium flow rates of 20–300 mL $min^{-1}$. Oxygen permeation fluxes through the membranes were calculated from the effluent flow rate and the concentration of oxygen in the effluent. The leakage was <1% in all the oxygen permeation experiments, and was subtracted when calculating the oxygen permeation fluxes.

## Results and Discussion

### *Determination of permeation resistance parameters*

BSCF, a popular mixed conducting material, has been investigated thoroughly as oxygen permeable membranes[21,24–29] and cathodes of SOFCs recently.[4] It was chosen as a typical material for this report, because its transport properties have been well addressed. Two membranes with different thicknesses were evaluated by the model over a wide range of variables. To determine the three parameters in Eqs. 27 and 28, one side of the oxygen partial pressure was kept constant while changing the other side, and then the two interfacial exchange constants were obtained through linear regression. The relative errors were found to be no bigger than 2%. The bulk-permeation resistances, $r^b$, calculated from the two equations show small relative average errors in the range of 0.1–2.7%, and the average values were

**Table 1. Permeation Resistance Constants and Kinetic Parameters of BSCF Membrane at Various Temperatures**

| Temperature (°C) | $r_0'$ ($\times 10^3$ Ω cm$^2$) | $r_0''$ ($\times 10^3$ Ω cm$^2$) | $r^b$ ($\times 10^3$ Ω cm$^2$) | $k_0'$ ($\times 10^4$ cm s$^{-1}$) | $k_0''$ ($\times 10^4$ cm s$^{-1}$) | $D_s$ ($\times 10^6$ cm$^2$ s$^{-1}$) |
|---|---|---|---|---|---|---|
| 940 | 6.86 | 1.69 | 15.7 | 6.08 | 24.7 | 13.3 |
| 900 | 7.17 | 1.73 | 19.3 | 5.63 | 23.3 | 10.5 |
| 900* | 6.63 | 2.28 | 40.6 | 6.09 | 17.7 | 9.94 |
| 850 | 7.56 | 2.05 | 27.9 | 5.11 | 18.9 | 6.92 |
| 800 | 7.80 | 3.04 | 40.2 | 4.73 | 12.1 | 4.59 |
| 750 | 10.2 | 4.01 | 62.3 | 3.45 | 8.78 | 2.83 |
| 715 | 12.3 | 6.41 | 81.7 | 2.76 | 5.30 | 2.08 |
| 680 | 16.5 | 8.08 | 114 | 1.99 | 4.06 | 1.44 |

*The data in the column obtained on 1.0 mm BSCF membrane.

used for the modeling investigation. Experimental measurements of total permeation resistance, $r^{tot}$, for the 0.5-mm BSCF membrane plotted against oxygen partial pressure on each side are shown in Figure 2. It reveals that the model Eqs. 27 and 28 are an excellent match to the experimental data with correlation coefficient larger than 0.997.

The applicability of the model with the parameters listed in Table 1 was investigated by applying the parameters to model another membrane with a thickness of 1.0 mm. Figure 3 shows the dependence of oxygen flux on oxygen partial pressure on each side at 900°C. As shown in Figure 3, the model data are a little higher than the experimental data by a factor of 1.05. The surface morphologies and microstructure (such as grains boundaries, impurities, gas pore, and grain size) of perovskite membranes have big influences on oxygen permeation.[24,25] Although the preparation procedures are the same, it still cannot guarantee the identical surface morphologies and microstructure for membranes. Considering the modest difference from one membrane to another, the model gives a good prediction. Table 1 lists the three parameters obtained on the 1.0-mm membrane at 900°C. The interfacial exchange resistance at the interfacial I is a little smaller than that of the 0.5-mm membrane, but the resistance constant at the interfacial II shows a slightly larger value. After normalized by dividing by the thickness, the small difference between the bulk-permeation resistances may be promoted by the different microstructures of the two membranes.

### *Kinetic parameters*

The interfacial exchange kinetic constants, $k_0'$ and $k_0''$, can be calculated through Eqs. 25 and 26. For the BSCF perovskite oxide, the electronic conductivity is far higher than its ionic conductivity. Therefore, the bulk-transport resistance, $r^b$, is dominated by the oxygen ionic transport resistance, $r^b_{O^{2-}}$. Combining Eqs. 8 and 30 gives

$$D_s = \frac{RT}{4F^2 C_{O^{2-}}} \frac{L}{r^b_{O^{2-}}} \tag{33}$$

In the literature, a few studies on the oxygen nonstoichiometry ($\delta$) of BSCF are available.[30–33] The value of $\delta$ has a similar dependence on the oxygen partial pressure and temperature, typically found in the range of 0.35–0.65. Here, $\delta = 0.5$ was adopted to calculate the kinetic constants in the investigated temperatures without causing significant errors. The calculated kinetic constants are listed in Table 1. If the two interfaces have the same exchange constants, the $r''$ would be far larger than $r'$ due to $P^{II}_{O_2} << P^{I}_{O_2}$, so $r'$ cannot significantly affect the oxygen permeation through membranes. However, many experimental results show that the porous active coating layer on feed side can effectively improve the oxygen fluxes for perovskite membranes,[28,34,35] which means that $r'$ makes a big contribution to the total resistance. For example, Tan et al. reported that the oxygen flux was increased by ~300% at 900°C for a $La_{0.6}Sr_{0.4}Co_{0.2}Fe_{0.8}O_3$ (LSCF) hollow fiber membrane modified by a LSCF porous layer on the feed side.[34] In our earlier research, we found that the oxygen flux was improved by 40–100% at 940°C for a $BaCe_{0.15}Fe_{0.85}O_3$ membrane coated by a BSCF porous layer on the feed side.[35] These results suggest that under oxygen permeation process, the two interfaces have different exchange constants, and oxygen exchange kinetics on interface II is faster than that of on interface I. The difference may be a result of the microstructure developing on interfaces during oxygen permeation. Many researchers have found that perovskite membranes have different surface morphologies on both sides after permeation tests.[36–38] As listed in Table 1, the exchange constants of interface II are several times larger than those of the interface I. That is to say, oxygen exchange rates on interface II are faster than those on interface I under the same oxygen partial pressure.

The kinetic parameters of BSCF have been widely investigated with many methods and by different researchers. However, the kinetic parameters shown in the literature are chemical diffusion coefficients, vacancy diffusion coefficients, tracer diffusion coefficients, or self-diffusion coefficients obtained by different methods. Here, for the comparison purpose, the chemical diffusion coefficients and vacancy diffusion coefficients are converted to self-diffusion coefficients according to Ref. 27. The chemical exchange coefficients were treated similarly. The kinetic parameters obtained in this work are summarized in Table 2 and are

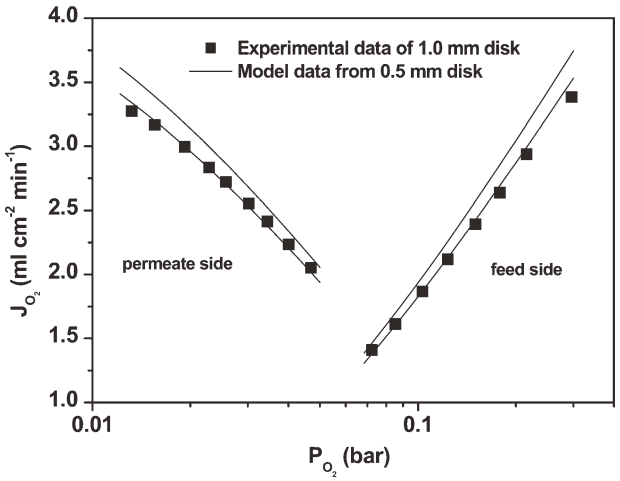


**Figure 3. Comparison of model data from 0.5-mm disk with the experimental data of 1.0-mm disk at 900°C.**

**Table 2. Comparison of Kinetic Parameters Obtained in This Work with Literature Data**

| Method | Temperature (°C) | Exchange Coefficient ($\times 10^4$ cm $s^{-1}$) | Self-Diffusion Coefficient ($\times 10^6$ $cm^2$ $s^{-1}$) | Ref. |
|---|---|---|---|---|
| Oxygen permeation | 800 | $k'_{ex} = 2.1$, $P_{O_2} = 0.21$ bar<br>$k''_{ex} = 5.4$, $P_{O_2} = 0.21$ bar | $D_s = 4.59$ | This work |
| Oxygen permeation* | 700 | $k'_{ex} = 1.1$, $P_{O_2} = 0.21$ bar<br>$k''_{ex} = 2.3$, $P_{O_2} = 0.21$ bar | $D_s$ =1.77 | This work |
| Oxygen permeation | 700 | | $D_s = 1.6$ | 30 |
| Conductivity relaxation | 700 | $k_{red} = 0.094$, $P_{O_2} = 0.021$ bar<br>$k_{ox} = 0.17$, $P_{O_2} = 0.009$ bar | $D_s = 0.06$ | 27 |
| Conductivity relaxation | 800 | $k_{red} = 3.5$, $P_{O_2} = 1.01$ bar<br>$k_{ox} = 4.6$, $P_{O_2} = 0.334$ bar | $D_s = 3.0$ | 40 |
| Tracer diffusion† | 700 | $k^*$ =1.3, $P_{O_2} = 0.5$ bar | $D^* = 0.8$ | 39 |

$k_{red}$ and $k_{ox}$ correspond to the interfacial exchange constants of reduction of oxygen molecules and oxidation of oxygen ions, respectively.
*The data in the column calculated from the linear relationship shown in Figure 6.
†The data obtained on a dense BSCF thin film.

compared with the converted literature data. It is found that the interfacial exchange parameters are similar, if they are obtained under the same oxygen partial pressure. The big discrepancies between diffusion coefficients may be related to the phase transformation from cubic to hexagonal at intermediate temperatures.[40] Regarding the different experimental methods listed in Table 2, it should be pointed out that conductivity relaxation and tracer diffusion experiments were performed in thermal equilibrium, whereas the oxygen permeation was studied under permeation steady state. Therefore, the kinetic parameters obtained under permeation steady states are more useful for practical applications in the field of MIEC membranes and SOFCs.

### *Influences of temperature*

After the three parameters were determined, the three permeation resistances through the membrane can be calculated under a certain oxygen partial pressure on each side. Figure 4 shows the effects of temperature on the distribution of resistances. It reveals the share of each component of the total permeation resistance and shows which step would be the r.d.s. As shown in the figure, the share of $r'$ increases with the temperature, whereas the share of $r^b$ decreases with the increase of temperature, and as a result the share of $r''$ remains almost constant during the change of temperature. As shown in Figure 4, with the increase of temperature the permeation r.d.s. gradually shifts from predominantly bulk-diffusion limitation to interfacial exchange limitation under an oxygen partial pressure gradient of 0.21 bar/0.02 bar.

For perovskite membranes, it is commonly found that the apparent activation energies for oxygen permeation show a two-stage phenomenon. The activation energies at the high-temperature stage are usually smaller than those at low-temperature stage. For example, LSCF shows a smaller activation energy (91 kJ $mol^{-1}$) when the temperature is higher than 880°C, and a larger value (153 kJ $mol^{-1}$) when the temperature is in the range of 750–850°C.[17] The change of activation energy was regarded as the r.d.s. shifting from predominantly bulk diffusion to predominantly interfacial exchange during cooling down. For BSCF membranes, the change of activation energies has also been reported by many researchers. Typically, the transition temperature is in the range of 750–800°C. For example, Shao et al. found that the permeation activation energy is 40.9 kJ $mol^{-1}$ in the range of 775–950°C and 72.6 kJ $mol^{-1}$ in the range of 600–775°C.[21] Figure 5 shows the Arrhenius plots of oxygen permeation through the BSCF membrane. The data points marked as solid circles are calculated from the resistance constants of bulk diffusion, which reveal the ideal permeation fluxes, if there is no influence of interfacial exchange. For the real permeation process, the permeation fluxes are marked as solid squares and lower than the ideal permeation fluxes. The two-stage activation energies shown in the figure are similar to those reported in the literature except a little difference, which is produced by the different methods used for the measurement. Here, the activation energies were obtained under a fixed oxygen partial gradient 0.21 bar/0.02 bar, whereas others in the literature were detected usually under fixed flow rate sweep gas.

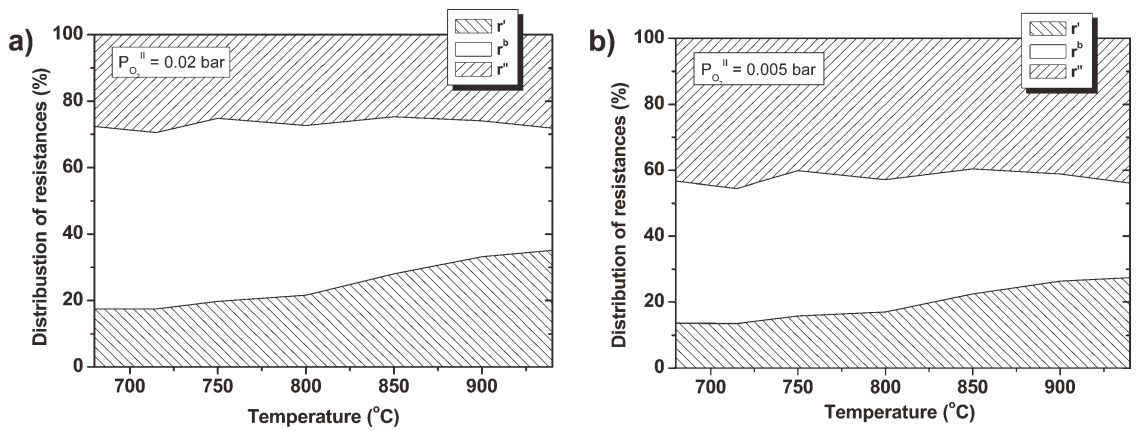


**Figure 4. Effects of temperature on distribution of permeation resistances.**

**Feed side: $P^{I}_{O_2} = 0.21$ bar; permeation side: (a) $P^{II}_{O_2} = 0.02$ and (b) $P^{II}_{O_2} = 0.005$ bar.**

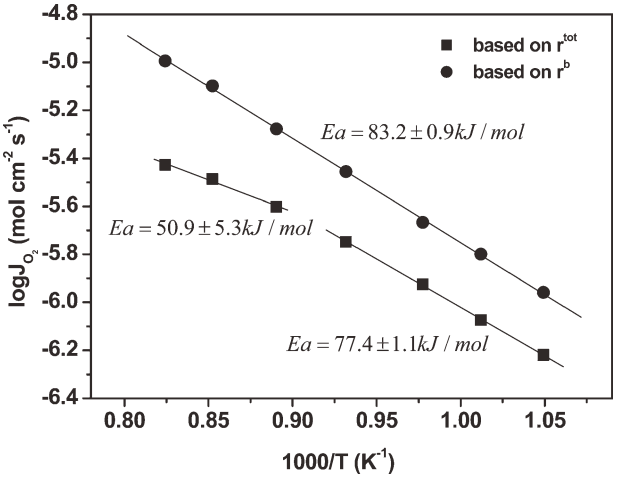


**Figure 5. Arrhenius plots of oxygen permeation fluxes of the 0.5-mm BSCF membrane under oxygen partial pressure gradient of 0.21 bar/0.02 bar.**

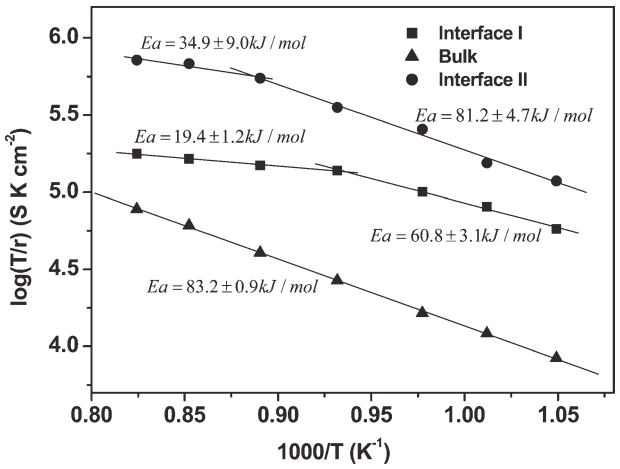


**Figure 6. Activation energies of interfacial resistance constant $r_0'$, $r_0''$ and bulk-resistance constant $r^b$ under oxygen partial pressure gradient of 0.21 bar/0.02 bar.**

Figure 6 shows the activation energies of the interfacial resistance constants $r_0'$ and $r_0''$, and the bulk-resistance constant $r^b$. As shown in the figure, the two interfacial resistance constants show lower activation energies at the high-temperature stage and higher values at lower temperature. However, the activation energy of the bulk-resistance constant does not change over a wide-temperature range (680–940°C), and gives 83.2 ± 0.9 kJ mol$^{-1}$. That is to say, the change of apparent activation energies as a function of temperature for BSCF membrane is due to the r.d.s. shifting from predominantly interfacial exchange to predominantly bulk diffusion. Hong and Choi also found the activation energies of BSCF at high temperature were lower than those at low temperature. They found that the activation energy for bulk diffusion is bigger than that for interfacial exchange at high temperature.[41] This conclusion matches very well with the results obtained by our model. In addition, higher activation energy was reported for the bulk diffusion (86 ± 8 kJ mol$^{-1}$) than that for the exchange kinetics (64 ± 12 kJ mol$^{-1}$) in temperature range of 550–750°C measured by electrical conductivity relaxation method.[27] The two values are all closed to those obtained through the model. For the investigated BSCF membrane, the $L_c$ values defined by Eq. 32 decrease gradually from 0.86 mm at 940°C to 0.44 mm at 680°C under an oxygen partial pressure gradient of 0.21 bar/0.02 bar. This phenomenon also was verified by other researchers.[41] However, the changes of activation energies of the two interfacial resistance constants are still not clear. Because the interfacial exchange process includes several steps, such as adsorption, dissociation, charge transfer, surface diffusion, and oxygen ions merging into lattices, it is difficult to identify which step is the r.d.s. even if it is assumed that the interfaces are not affected by the change of temperature.

### *Influences of membrane thickness*

Figure 7 shows the distribution of permeation resistances across the BSCF membranes when the thickness is reduced from 10 mm to 10 $\mu$m. As expected, the share of $r^b$ decreases with the reduction of membrane thickness. The interfacial exchange process becomes the dominant steps when the thickness is less than ~0.6 mm. Further, reducing the thickness can marginally improve the permeation fluxes, as shown in Figure 8. That is why, there is previously no report that the permeation fluxes exceed 10 mL cm$^{-2}$ min$^{-1}$ through unmodified BSCF membranes. Recently, Leo et al. reported a BSCF hollow fiber membrane with high-permeation flux but still smaller than 10 mL cm$^{-2}$ min$^{-1}$, unless there are Pt nanoparticles as oxygen exchange catalysts being coated on both sides.[42] If there is no influence of interfacial exchange on permeation, just like the dash line shown in the figure, the flux increase linearly with the reduction of membrane thickness. In addition, the line reveals the upper limit of oxygen fluxes through BSCF membranes at 900°C and under the oxygen partial pressure gradient of 0.21 bar/0.02 bar. It can be expected that the BSCF membrane has permeation fluxes compared with microporous membranes, when the thickness is reduced to less than 100 $\mu$m, if there is no support layer controlling the mass transport between the dense layer and atmosphere.

### *Influences of oxygen partial pressure*

The oxygen partial pressure on each side of the membrane has great influences on oxygen permeation process, which not only affect the oxygen chemical gradient (or total permeation driving

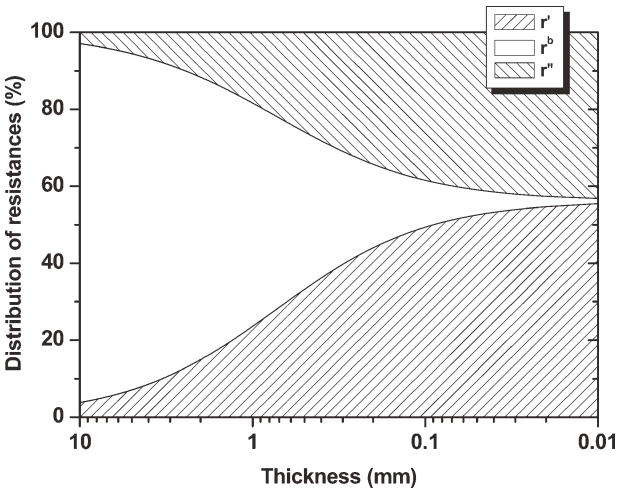


**Figure 7. The dependence of distribution of permeation resistances on membrane thickness across the BSCF membranes at 900°C.**

**Oxygen partial pressure of feed and permeation sides are 0.21 and 0.02 bar, respectively.**

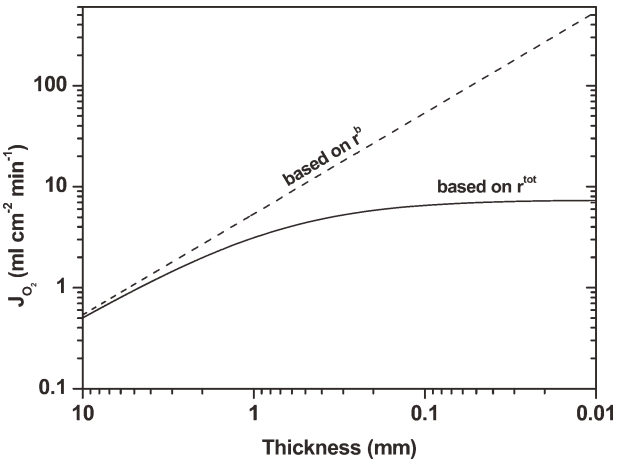


**Figure 8. Influences of membrane thickness on oxygen permeation fluxes of BSCF membrane at 900°C.**

**Oxygen partial pressure of feed and permeation sides are 0.21 and 0.02 bar, respectively.**

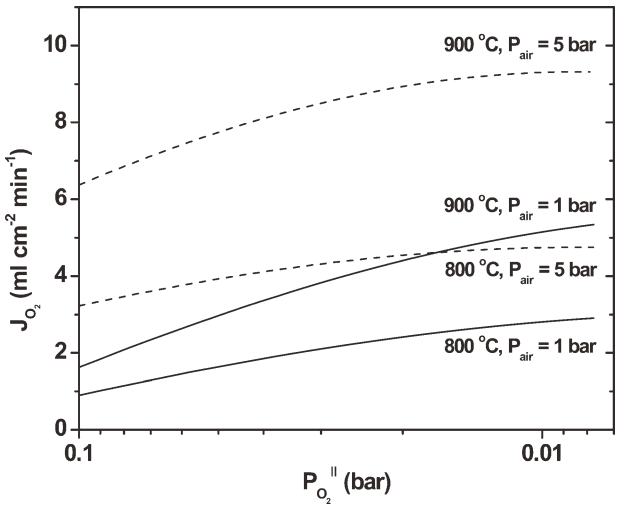


**Figure 9. Dependence of oxygen fluxes on oxygen partial pressure of permeation side of the 0.5-mm BSCF membrane at 800 and 900°C.**

force) across the membrane but also oxygen exchange kinetics at interfacial zones. The dependence of oxygen fluxes on oxygen partial pressure of permeation side is plotted in Figure 9, and corresponding distribution of permeation resistances exerted by the individual permeation steps is shown in Figure 10. Under a certain feed oxygen pressure, the permeation flux increases with the reduction of $P_{O_2}^{II}$. At the same time, $r''$ increases with the decrease of $P_{O_2}^{II}$, as shown in Figure 10. The share of $r''$ at 800°C is about 15% at $P_{O_2}^{II} = 0.1$ bar, gradually increasing to about 40% at $P_{O_2}^{II} = 0.007$ bar. The reduction of $P_{O_2}^{II}$ can enhance the total driving force across membranes, but the increment can be completely consumed by the increased resistance at interface II. Finally, the permeation flux can only be marginally improved for the 0.5 mm BSCF membrane by further decreasing $P_{O_2}^{II}$. This

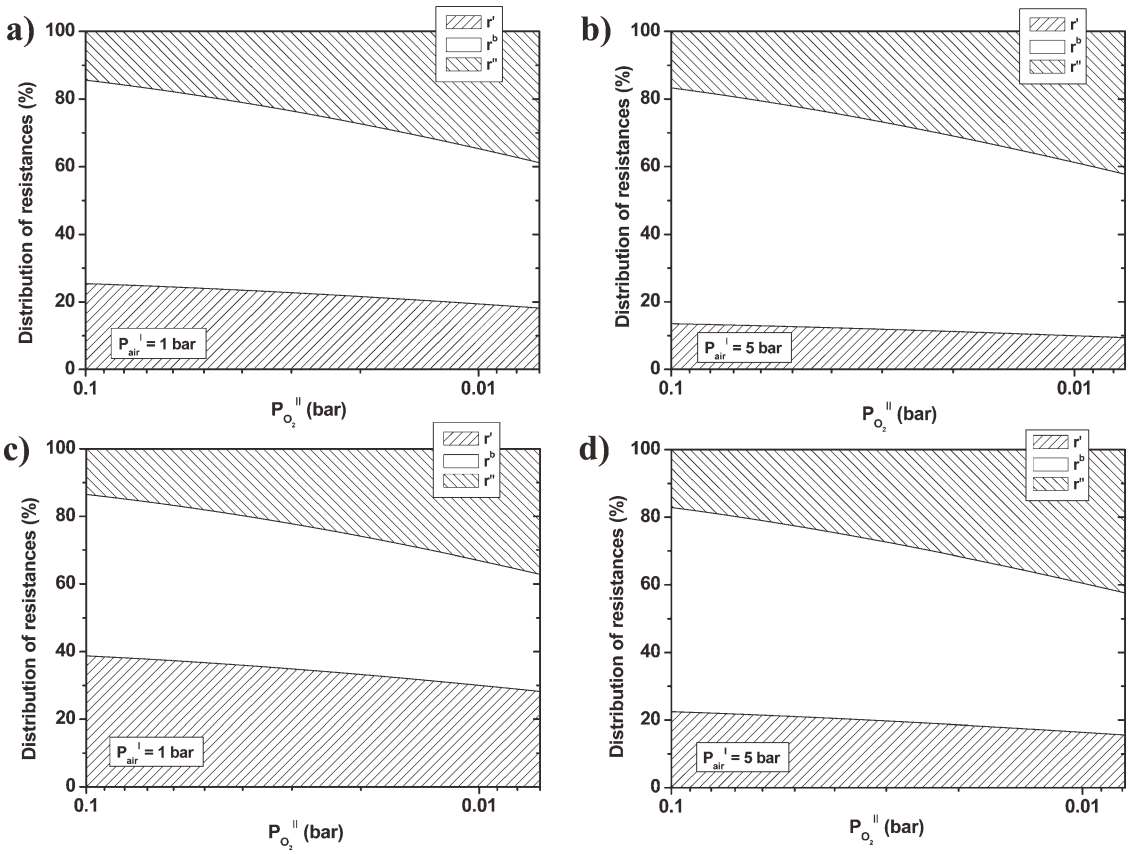


**Figure 10. Distribution of permeation resistances across the 0.5-mm BSCF membrane under various oxygen partial pressures of permeation side.**

**(a) and (b) 800°C and (c) and (d) 900°C.**

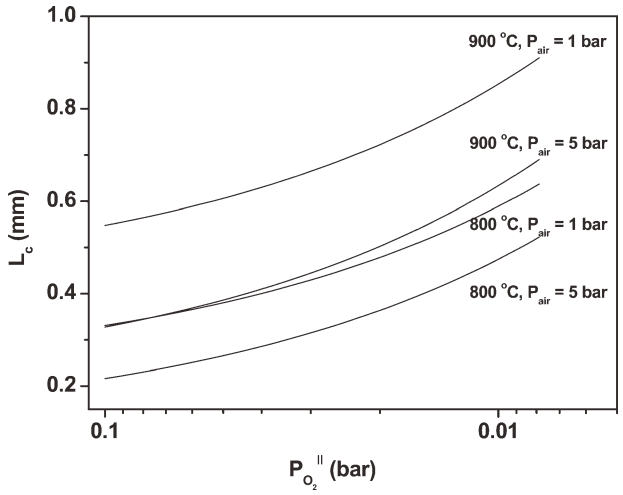


**Figure 11. Influence of oxygen partial pressure of permeation side on characteristic thickness of BSCF membrane at 800 and 900°C.**

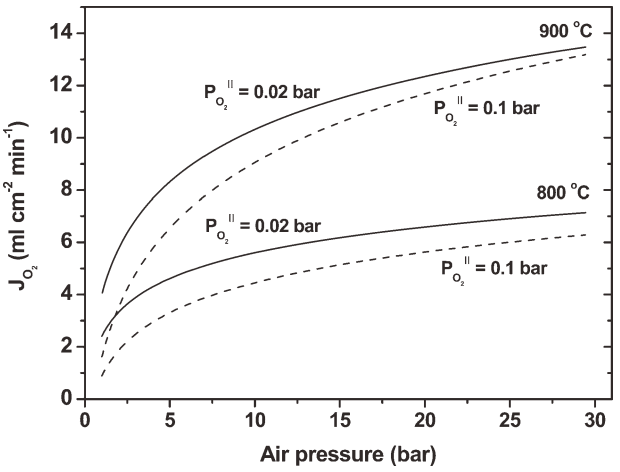


**Figure 12. Dependence of oxygen fluxes on oxygen partial pressure of feed side of the 0.5-mm BSCF membrane at 800 and 900°C.**

trend remains unchanged with the alteration of temperature and feed pressure. As expected, the characteristic thickness, $L_c$, increases with the decrease of $P^{II}_{O_2}$ (Figure 11).

For a real air separation process, the membranes should be operated at high-feed pressures for economic considerations. However, it is difficult to obtain such experimental data in laboratories, because the sealing of membranes at high temperatures and high pressures is still a big problem up to now.[29] Therefore, it is interesting and necessary to predict the oxygen permeation performance of BSCF membranes at high-operating pressures using model approach. To do this, here we need to assume that the three resistance constants do not change significantly at high pressure. Figure 12 shows the prediction by the model of changes in the oxygen partial pressure at the feed side under oxygen gradients of high-pressure air ($C_{O_2}$ = 21%) vs. helium

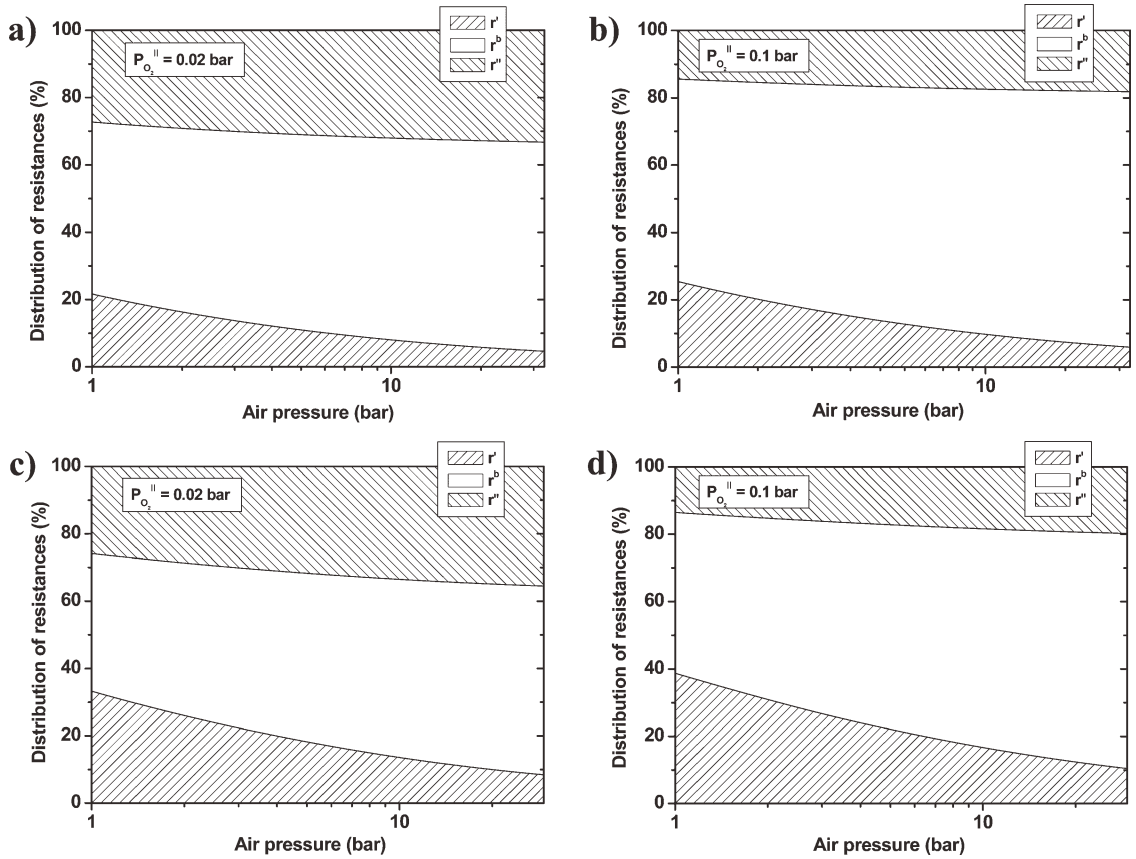


**Figure 13. Distribution of permeation resistances across the 0.5-mm BSCF membrane under various oxygen partial pressures of feed side.**

**(a) and (b) 800°C and (c) and (d) 900°C.**

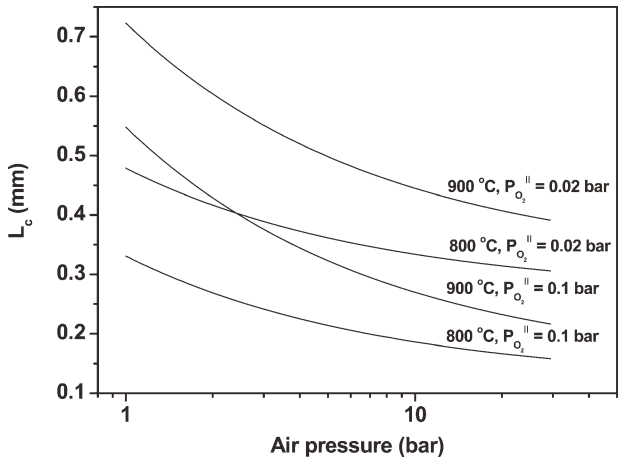


**Figure 14. Influence of oxygen partial pressure of feed side on characteristic thickness of BSCF membrane at 800 and 900°C.**

($P_{O_2}$ = 0.02 or 0.1 bar), and the corresponding distribution of permeation resistances is shown in Figure 13. As observed in Figure 12, the oxygen permeation flux increases quickly in the air pressure range of 1–5 bar, then slowly with further increase of pressure, and finally can be marginally improved when the air pressure is greater than 20 bar. This modeling result agrees with the our previous experimental and model findings on tubular BSCF membranes.[29,43] From Figure 12, one can find that the difference of oxygen flux brought by the two permeation oxygen pressures becomes smaller during the enhancement of air pressure, especially for the membrane operated at higher temperature. The permeation resistance $r'$ decreases quickly with the increase of air pressure; and under a higher permeation oxygen pressure (0.1 bar), $r'$ decreases more quickly, as shown in Figure 13. That is to say, increasing the air pressure does not only improve the driving force across the membrane but also make less oxygen chemical potential consumed by the interfacial exchange at zone I. The characteristic thickness, $L_c$, as shown in Figure 14, decreases quickly with the increase of air pressure, which is attributed to the reduction of permeation resistance $r'$. From Figures 11 and 14, one can clearly see that $L_c$ is a process parameter affected by oxygen partial pressures across membranes and operating temperature. The thickness of the investigated BSCF membrane is 0.5 mm. If $L_c$ is larger than 0.5 mm under a certain condition, the permeation process is mainly controlled by interfacial exchange; similarly, if $L_c$ is smaller than 0.5 mm, the permeation process is mainly controlled by bulk diffusion. All the information is reflected by Figures 11 and 14 with the changes of oxygen partial pressures and temperature.

## Conclusions

A simple oxygen permeation model for mixed conducting membranes has been developed, which can well describe the permeation fluxes. The model parameters can be easily solved by measuring oxygen fluxes as functions of oxygen partial pressures on both sides of the membrane and operating temperature. The obtained three resistance constants can be used to calculate kinetics constants, including interfacial exchange constants and the oxygen ionic self-diffusion coefficient. The different interfacial exchange constants of the two interfaces obtained through the model agree with many reported experimental results. With this model, the oxygen permeation resistances across membranes can be distinguished, and a map of the resistance distribution can be drawn. The results of this model indicate that the activation energy of bulk diffusion is 83.2 ± 0.9 kJ mol$^{-1}$ in a wide-temperature range, and this value is close to the data obtained using the conductivity relaxation method. The two interfacial exchange processes have different activation energies and show a two-stage behavior, but are both smaller than that of bulk diffusion. The interfacial exchange activation energies at higher temperature are smaller than those at lower temperature. The discrepancy in activation energies for interfacial exchange and bulk diffusion leads to the apparent activation energies of oxygen permeation through BSCF showing a two-stage phenomenon.

The influences of membrane thickness and oxygen partial pressure of both sides on the oxygen permeation of the BSCF membrane were investigated. The interfacial exchange process becomes the predominant step when increasing the operating temperature or decreasing the thickness of the membrane. Further improvement of the permeation flux by decreasing membrane thickness must be accompanied with surface modification, such as coating active porous layers on both sides. On the basis of permeation resistance analysis, it has been determined that the interfacial resistances are greatly influenced by the oxygen partial pressure. To enhance the permeation driving force by decreasing $P^{II}_{O_2}$ results in the increase of total resistance and share of $r''$. However, to enhance driving force by increasing $P^{I}_{O_2}$ leads to the reduction of total resistance and share of $r'$. A low-permeation oxygen pressure is unnecessary, if the membrane is operated under a high-feed air pressure. Altering the operating parameters, including temperature, and oxygen partial pressure on each side, can make the r.d.s. shifted from predominantly bulk diffusion to predominantly interfacial exchange. Finally, with this model, one can clearly know which step is the important step and how much the oxygen permeation process controlled by the steps, and know what kind of strategies (for instance, decreasing membrane thickness, reducing $P^{II}_{O_2}$ or rising $P^{I}_{O_2}$) would be effective to improve the oxygen flux.

## Acknowledgments

The authors gratefully acknowledge the financial support of National Natural Science Foundation (20801053), National Natural Science Foundation for Distinguished Young Scholars of China (20725313), and Director Foundation of State Key Laboratory of Catalysis (R201010).

## Notation

$C_{O^{2-}}$ = volume concentration of oxygen anions at equilibrium
$D^*$ = tracer diffusion coefficient
$D_s$ = self-diffusion coefficient of oxygen ions
$e$ = electronic charge
$F$ = Faraday constant
$j_{ex}$ = balance exchange rate
$j_{O_2}$ = oxygen permeation flux
$k_B$ = Boltzmann constant
$k_{ex}$ = equilibrium interfacial exchange coefficient
$k_0$ = equilibrium interfacial exchange coefficient at oxygen partial pressure of 1 bar
$I_e$ = electronic current density
$I_{O^{2-}}$ = oxide ionic current density
$l$ = thickness of interface layers or membrane bulk
$L$ = thickness of membrane
$L_c$ = characteristic thickness
$n$ = a positive number
$P_{O_2}$ = partial pressure of molecular oxygen
$P_0$ = oxygen partial pressure equals to 1 bar
$r$ = area specific resistance of species $i$
$r_0$ = area specific resistance at oxygen partial pressure of 1 bar
$R$ = gas constant
$T$ = temperature

### Greek letters

$\delta$ = oxygen nonstoichiometry
$\kappa_i$ = specific conductance of species $i$
$\Delta\mu_i$ = chemical potential deference of species $i$ across the membrane
$\mu_i$ = chemical potential of species $i$
$\sigma_i$ = conductivity of species $i$

### Superscripts

$b$ = membrane bulk
I = gas phase of feed side
II = gas phase of permeation side
tot = including both interfaces and membrane bulk
$'$ = interface I
$''$ = interface II

## Literature Cited


1. Teraoka Y, Zhang HM, Furuka S, Yamazoe N. Oxygen permeation through perovskite-type oxides. *Chem Lett*. 1985;11:1743–1746.
2. Kharton VV, Naumovich EN, Nikolaev AV. Materials of high-temperature electrochemical oxygen membranes. *J Membr Sci*. 1996; 111:149–157.
3. Sunarso J, Baumann S, Serra JM, Meulenberg WA, Liu S, Lin YS, Diniz da Costa JC. Mixed ionic–electronic conducting (MIEC) ceramic-based membranes for oxygen separation. *J Membr Sci*. 2008; 320:13–41.
4. Shao ZP, Haile SM. A high-performance cathode for the next generation of solid-oxide fuel cells. *Nature*. 2004;431:170–173.
5. Dusastre V, Kilner JA. Optimisation of composite cathodes for intermediate temperature SOFC applications. *Solid State Ionics*. 1999;126:163–174.
6. Serra JM, Vert VB, Buchler O, Meulenberg WA, Buchkremer HP. IT-SOFC supported on mixed oxygen ionic–electronic conducting composites. *Chem Mater*. 2008;20:3867–3875.
7. Yang WS, Wang HH, Zhu XF, Lin LW. Development and application of oxygen permeable membrane in selective oxidation of light alkanes. *Top Catal*. 2005;35:155–167.
8. Liu YY, Tan XY, Li K. Mixed conducting ceramics for catalytic membrane processing. *Catal Rev Sci Eng*. 2006;48:145–198.
9. Akin FT, Lin YS. Oxidative coupling of methane in dense ceramic membrane reactor with high yields. *AIChE J*. 2002;48:2298–2306.
10. Zhu XF, Yang WS. Mixed conductor oxygen permeable membrane reactors. *Chin J Catal*. 2009;30:801–816.
11. Zeng Q, Zu YB, Fan CG, Chen CS. $CO_2$-tolerant oxygen separation membranes targeting $CO_2$ capture application. *J Membr Sci*. 2009; 335:140–144.
12. Smart S, Lin CXC, Ding L.Thambimuthu K.Diniz da Costa JC. Ceramic membranes for gas processing in coal gasification. *Energy Environ Sci*. 2010;3:268–278.
13. Bouwmeester HJM, Burggraaf AJ. *Dense ceramic membranes for oxygen separation*. In: Gellings PJ, Bouwmeester HJM, editors. *The CRC Handbook of Solid State Electrochemistry*. CRC: Boca Raton, 1997:481–553.
14. Kim S, Yang YL, Jacobson AJ, Abeles B. Oxygen surface exchange in mixed ionic electronic conductor membranes. *Solid State Ionics*. 1999;121:31–36.
15. Lee TH, Yang YL, Jacobson AJ, Abeles B, Zhou M. Oxygen permeation in dense $SrCo_{0.8}Fe_{0.2}O_{3-\delta}$ membranes: surface exchange kinetics versus bulk diffusion. *Solid State Ionics*. 1997;100:77–85.
16. Kim S, Yang YL, Jacobson AJ, Abeles B. Diffusion and surface exchange coefficients in mixed ionic electronic conducting oxides from the pressure dependence of oxygen permeation. *Solid State Ionics*. 1999;106:189–195.
17. Xu SJ, Thomson WJ. Oxygen permeation rates through ion-conducting perovskite membranes. *Chem Eng Sci*. 1999;54:3839–3850.
18. Lin YS, Wang WJ, Han J. Oxygen permeation through thin mixed-conducting solid oxide membranes. *AIChE J*. 1994;40:786–798.
19. Virkar AV. Theoretical analysis of the role of interfaces in transport through oxygen ion and electron conducting membranes. *J Power Sources*. 2005;147;8–31.
20. Bouwmeester HJM, Burggraaf AJ. Importance of the surface exchange kinetics as rate limiting step in oxygen permeation through mixed-conducting oxides. *Solid State Ionics*. 1994;72:185–194.
21. Shao ZP, Yang WS, Cong Y, Dong H, Tong JH, Xiong GX. Investigation of the permeation behavior and stability of a $Ba_{0.5}Sr_{0.5}$ $Co_{0.8}Fe_{0.2}O_{3-\delta}$ oxygen membrane. *J Membr Sci*. 2000;172:177–188.
22. Zhu XF, Cong Y, Yang WS. Oxygen permeability and structural stability of $BaCe_{0.15}Fe_{0.85}O_{3-\delta}$ membranes. *J Membr Sci*. 2006;283: 38–44.
23. Zhu XF, Yang WS. Composite membrane based on ionic conductor and mixed conductor for oxygen permeation. *AIChE J*. 2008;54: 665–672.
24. Tan L, Gu XH, Yang L, Zhang LX, Wang CQ, Xu NP. Influence of sintering condition on crystal structure, microstructure, and oxygen permeability of perovskite-related type $Ba_{0.5}Sr_{0.5}Co_{0.8}Fe_{0.2}O_{3-\delta}$ membranes. *Sep Purif Technol*. 2003;32:307–312.
25. Wang HH, Tablet C, Feldhoff A, Caro H. Investigation of phase structure, sintering, and permeability of perovskite-type $Ba_{0.5}Sr_{0.5}$ $Co_{0.8}Fe_{0.2}O_{3-\delta}$ membranes. *J Membr Sci*. 2005;262:20–26.
26. Girdauskaite E, Ullmann H, Vashook VV, Guth U, Caraman GB, Bucher E, Sitte W. Oxygen transport properties of $Ba_{0.5}Sr_{0.5}$ $Co_{0.8}Fe_{0.2}O_{3-\delta}$ and $Ca_{0.5}Sr_{0.5}Mn_{0.8}Fe_{0.2}O_{3-x}$ obtained from permeation and conductivity relaxation experiments. *Solid State Ionics*. 2008;179:385–392.
27. Bucher E, Egger A, Ried P, Sitte W, Holtappels P. Oxygen nonstoichiometry and exchange kinetics of $Ba_{0.5}Sr_{0.5}Co_{0.8}Fe_{0.2}O_{3-\delta}$. *Solid State Ionics*. 2008;179:1032–1035.
28. Wang Y, Hao H, Jia J, Yang D, Hu X. Improving the oxygen permeability of $Ba_{0.5}Sr_{0.5}Co_{0.8}Fe_{0.2}O_{3-\delta}$ membranes by a surface-coating layer of $GdBaCo_2O_{5+\delta}$. *J Eur Ceram Soc*. 2008;28:3125–3130.
29. Zhu XF, Sun SM, Cong Y, Yang WS. Operation of perovskite membrane under vacuum and elevated pressures for high-purity oxygen production. *J Membr Sci*. 2009;345:47–52.
30. Wang HH, Cong Y, Yang WS. Oxygen permeation study in a tubular $Ba_{0.5}Sr_{0.5}Co_{0.8}Fe_{0.2}O_{3-\delta}$ oxygen permeable membrane. *J Membr Sci*. 2002;210:259–271.
31. Vente JF, McIntosh S, Haije WG, Bouwmeester HJM. Properties and performance of $Ba_xSr_{1-x}Co_{0.8}Fe_{0.2}O_{3-\delta}$ materials for oxygen transport membranes. *J Solid State Electrochem*. 2006;10:581–588.
32. Girdauskaite E, Ullmann H, Daroukh M, Vashook V, Bülow M, Guth U. Oxygen stoichiometry, unit cell volume, and thermodynamic quantities of perovskite-type oxides. *J Solid State Electrochem*. 2007;11:469–477.
33. Kriegel R, Kircheisen R, Töpfer J. Oxygen stoichiometry and expansion behavior of $Ba_{0.5}Sr_{0.5}Co_{0.8}Fe_{0.2}O_{3-\delta}$. *Solid State Ionics*. 2010; 181:64–70.
34. Tan X, Wang Z, Liu H, Liu S. Enhancement of oxygen permeation through $La_{0.6}Sr_{0.4}Co_{0.2}Fe_{0.8}O_{3-\delta}$ hollow fiber membranes by surface modifications. *J Membr Sci*. 2008;324:128–135.
35. Zhu XF, Cong Y, Yang WS. Oxygen permeability and structural stability of $BaCe_{0.15}Fe_{0.85}O_{3-\delta}$ membranes. *J Membr Sci*. 2006;283: 38–44.
36. Li QM, Zhu XF, He YF, Yang WS. Oxygen permeability and stability of $BaCe_{0.1}Co_{0.4}Fe_{0.5}O_{3-\delta}$ oxygen permeable membrane. *Sep Purif Technol*. 2010;73:38–43.
37. Schlehuber D, Wessel E, Singheiser L, Markus T. Long-term operation of a $La_{0.58}Sr_{0.4}Co_{0.2}Fe_{0.8}O_{3-\delta}$-membrane for oxygen separation. *J Membr Sci*. 2010;351:16–20.
38. Alaee MA, Ghadimi A, Mohammadi T. Reinvestigation of the permeation behaviour of a $Ba_{0.5}Sr_{0.5}Co_{0.8}Fe_{0.2}O_{3\text{-delta}}$ perovskite-type membrane. *High Temp Mat Pr-Isr*. 2009;28:181–190.
39. Wang L, Merkle R, Maier J, Acartürk T, Starke U. Oxygen tracer diffusion in dense $Ba_{0.5}Sr_{0.5}Co_{0.8}Fe_{0.2}O_{3-\delta}$ films. *Appl Phys Lett*. 2009;94:1908–1903.
40. Yakovlev S, Yoo CY, Fang S, Bouwmeester HJM. Phase transformation and oxygen equilibration kinetics of pure and Zr-doped $Ba_{0.5}Sr_{0.5}Co_{0.8}Fe_{0.2}O_{3-\delta}$ perovskite oxide probed by electrical conductivity relaxation. *Appl Phys Lett*. 2010;96:254101–254103.
41. Hong WK, Choi GM. Oxygen permeation of BSCF membrane with varying thickness and surface coating. *J Membr Sci*. 2010;346:353–360.
42. Leo A, Smart S, Liu S, Diniz da Costa JC. High performance perovskite hollow fibres for oxygen separation. *J Membr Sci*. 2011;368: 64–68.
43. Wang HH, Wang R, Liang DT, Yang WS. Experimental and modeling studies on $Ba_{0.5}Sr_{0.5}Co_{0.8}Fe_{0.2}O_{3-\delta}$ (BSCF) tubular membranes for air separation. *J Membr Sci*. 2004;243:405–415.


*Manuscript received Jan. 24, 2011, revision received Apr. 3, 2011, and final revision received Jun. 16, 2011.*